PHYSICAL REVIEW D

PARTICLES AND FIELDS

THIRD SERIES, VOLUME 33, NUMBER 5 1 MARCH 1986

Measurement of the $\pi \to e\nu$ branching ratio

D. A. Bryman,* R. Dubois,*,† J. A. Macdonald, T. Numao, B. Olaniyi,*,‡
A. Olin,* and J.-M. Poutissou§
TRIUMF, Vancouver, British Columbia, Canada V6T 2A3

M. S. Dixit
National Research Council of Canada, Ottawa, Ontario, Canada K1A 0R6
(Received 15 October 1985)

A measurement of the $\pi \to e\nu$ branching ratio using a NaI(Tl) spectrometer yields a value $\Gamma((\pi \to e\nu)+(\pi \to e\nu\gamma))/\Gamma((\pi \to \mu\nu)+(\pi \to \mu\nu\gamma))=(1.218\pm0.014)\times10^{-4}$. The result is consistent with expectations of the standard electroweak theory incorporating electron-muon universality.

I. INTRODUCTION

The $\pi \to e\nu$ decay has long been of importance to the development of weak-interaction theory. Early interest in the decay stemmed from its role in the confirmation of the $(V-A)$ form of the universal Fermi interaction. As early as 1949, Ruderman and Finkelstein[1] had pointed out that a value of the branching ratio for $(\pi \to e\nu)/(\pi \to \mu\nu)$ of about 10^{-4} would indicate that the pion is a pseudoscalar particle and that π_{l2} decay is governed by axial-vector interactions. This assumed that the electron and the muon couple identically to the pion, an hypothesis now known as electron-muon $(e\text{-}\mu)$ universality in weak interactions. Under the assumption that the weak interaction contains only vector and axial-vector terms, the branching ratio is given by

$$\frac{\Gamma(\pi \to e\nu)}{\Gamma(\pi \to \mu\nu)} = \frac{m_e{}^2}{m_\mu{}^2}\frac{(m_\pi{}^2-m_e{}^2)^2}{(m_\pi{}^2-m_\mu{}^2)^2} = 1.28\times10^{-4}\,,$$

where $m_e c^2$, $m_\mu c^2$, and $m_\pi c^2$ are the electron, muon, and pion masses, respectively, and the $m_e{}^2/m_\mu{}^2$ helicity suppression term arises from the $(V-A)$ form of the interaction. In contrast, for a pure pseudoscalar interaction the branching ratio would be $(m_\pi{}^2-m_e{}^2)^2/(m_\pi{}^2-m_\mu{}^2)^2 \sim 5.4$, and for other forms of couplings, the decay would be forbidden. After some initial difficulties, the decay was observed[2] in 1958 in agreement with the phenomenological $(V-A)$ theory. With the subsequent establishment of the universal $(V-A)$ theory, $\pi \to e\nu$ decay could be examined as a sensitive test of electron-muon universality.

In the framework of the Weinberg-Salam-Glashow (WSG) electroweak theory, Marciano and Sirlin[3] showed that the value of the $\pi \to e\nu$ branching ratio including radiative corrections is

$$R = \frac{\Gamma((\pi \to e\nu)+(\pi \to e\nu\gamma))}{\Gamma((\pi \to \mu\nu)+(\pi \to \mu\nu\gamma))} = 1.233\times10^{-4}\,, \qquad (1)$$

in close agreement with early calculations by Berman[4] and Kinoshita[5] and was a consequence of gauge invariance. Further, the additional pion-structure-dependent radiative corrections to R were no larger than 0.3%. This was confirmed in specific model calculations by Goldman and Wilson.[6] Thus, the $\pi \to e\nu$ branching ratio provides a stringent test of $e\text{-}\mu$ universality in the context of the standard electroweak theory. Although universality for the third-generation lepton τ is best constrained by agreement between the calculated and measured τ lifetime,[7] the $\pi \to e\nu$ branching ratio remains the most sensitive test of universality among the three known lepton generations.

In the quark sector three or more generations are necessary in order to accommodate CP violation in the standard-model quark mixing matrix.[8] However, in the lepton sector there are still no compelling theoretical reasons for the existence of, or universality among the three generations; $e\text{-}\mu$ universality is built in and the lepton mixing matrix is diagonal due to the apparent masslessness of the neutrinos. Here, a search for rare lepton-flavor-violating reactions such as $\mu^- + \text{nucleus} \to e^- + \text{nucleus}$ or an accurate determination of the $\pi \to e\nu$ branching ratio R can serve to probe the relationship between generations.

Deviations from the predicted branching ratio (1) would signal the presence of new physics. For example, the deviations could be due to small pseudoscalar terms[9] found

in many extensions of the standard model which introduce new exotic particles. Because of interference between a pseudoscalar and the dominant axial-vector terms, the $\pi\to e\nu$ branching ratio is sensitive to terms proportional to $M_H{}^{-2}$, where M_H is the mass of the exotic particle that induces pseudoscalar terms in the interaction. This is in contrast with many still unobserved processes such as $\mu\to e\gamma$ for which the calculated rates are proportional to $M_H{}^{-4}$. Moreover, the sensitivity of the $\pi\to e\nu$ decay for exhibiting exotic new effects is enhanced because of the natural helicity suppression of the standard-model axial-vector contribution relative to the pseudoscalar term.

Maximal helicity suppression is effective only in the case of massless neutrinos. If neutrinos were massive, the weak-interaction eigenstates ν_a could be admixtures of mass eigenstates ν_i through a mixing matrix U_{ai}:

$$\nu_a=\sum U_{ai}\nu_i \ .$$

The $\pi\to e\nu$ decay would then be an incoherent sum of decay modes $\pi^+\to e^+\nu_i$. The measured branching ratio R would be affected and additional peaks would appear in the $\pi\to e\nu$ decay spectrum at energies determined by $m(\nu_i)$ as emphasized by Shrock.[10] The sensitivity to branches involving massive neutrinos would be increased by about 10^4 relative to the zero-mass neutrino case. Thus, the $\pi\to e\nu$ decay is an experimentally favored reaction with which to search for the existence of massive neutrinos. The results of the search for massive neutrinos based on the present work in the mass range of 4—135 MeV have been described previously.[11]

The first accurate measurement of R was performed by Anderson *et al.*[12] in 1958 using a double-focusing magnetic spectrometer. Positrons within a 10-MeV-wide energy window extending up to the maximum $\pi\to e\nu$ energy of 69.8 MeV were included to accept the inner bremsstrahlung radiative decays $\pi\to e\nu\gamma$. The measured branching ratio after correction for the unobserved low-energy $\pi\to e\nu\gamma$ positrons gave

$$R=(1.21\pm0.07)\times10^{-4}$$

in agreement with the theoretical value Eq. (1).

In 1964 another measurement of R using a 23-cm-diameter ×24-cm-long NaI(Tl) crystal was reported by Di Capua *et al.*[13] With a correction[14] for a subsequently improved measurement of the pion lifetime, their result based on 10 000 events was

$$R=(1.274\pm0.024)\times10^{-4} \ .$$

This value of R was (3.3±1.9)% away from the theoretical value (1). A new measurement of the branching ratio with improved precision performed[15] at TRIUMF is described below in detail.

II. EXPERIMENT

A. Method

To measure the branching ratio R, the 69.8-MeV positrons from the $\pi^+\to e^+\nu$ decay have to be detected in the presence of the 10^4 times more numerous positrons extending from 0—52.8 MeV that arise from the sequential decay process $\pi\to\mu\nu$, followed by $\mu\to e\bar{\nu}\nu$ (henceforth called the π-μ-e chain). A NaI(Tl) spectrometer is well suited to measure positrons over this wide energy range with good efficiency. The large π-μ-e chain component can be suppressed relative to $\pi\to e\nu$ events by limiting observation to approximately one pion lifetime ($\tau_\pi\sim26$ ns) which is short compared to the muon lifetime ($\tau_\mu\sim2200$ ns). The decay time distribution can also be measured for both $\pi\to e\nu$ and the π-μ-e chain events from which the $\pi\to e\nu$ and $\pi\to\mu\nu$ amplitudes can be obtained to calculate the branching ratio.

Using a method similar to that of Di Capua *et al.*,[13] energy spectra of positrons were collected during two identical time intervals, one beginning at time t_i after the pion stop and the second beginning at time t_i+t_s after the pion stop. The second interval essentially contained only positrons from the π-μ-e chain [$N(2)_{\pi\mu e}$] since t_s was long compared to the pion lifetime. However, the first interval contained events from both π-μ-e [$N(1)_{\pi\mu e}$] and $\pi\to e\nu$ [$N_{\pi e}$] origins. The branching ratio can then be expressed as

$$R=\left[\frac{\lambda_\mu}{\lambda_\pi-\lambda_\mu}\right]\frac{N_{\pi e}\{1-\exp[-(\lambda_\pi-\lambda_\mu)t_s]\}}{N(2)_{\pi\mu e}\exp(\lambda_\mu t_s)-N(1)_{\pi\mu e}} \ , \qquad (2)$$

where λ_π and λ_μ are the pion and muon decay constants, respectively. This procedure to measure R is independent of several important sources of possible systematic uncertainties including the positron detector solid angle, the muon contamination of the beam, the displacement t_i of the beginning of the first measurement interval with respect to the pion stop, and absolute widths of the two time intervals (as long as they are identical).

In an alternative method to measure R, decay time distributions of positrons from $\pi\to e\nu$ and the π-μ-e chain were measured from which amplitudes for the $\pi\to e\nu$ and $\pi\to\mu\nu$ components were obtained. The branching ratio is given by

$$R=\frac{A_{\pi\to e\nu}}{A_{\pi\to\mu\nu}} \ . \qquad (3)$$

B. Setup

The experimental setup is shown in Fig. 1. Positive pions of momentum 77±1 MeV/c were produced by a 500-MeV, 100-μA proton beam from the TRIUMF cyclotron striking a 1-cm-long carbon target viewed by the M13 low-energy pion channel. The beam was degraded by two plastic scintillation beam counters $B1$ and $B2$ and stopped in the inner three layers of a five-element scintillation-counter target ($B3$—$B7$) at a rate of 2×10^5 s^{-1}. The inset of Fig. 1 shows the details of the stopping counter. The dimensions of the scintillation counters used in the experiment are given in Table I. The beam size at counter $B1$ was 2 cm×2 cm. The muon and positron contaminations in the beam were each 10%. Pions were selected by their range and by their time of flight from the production target relative to a signal derived from the 23-MHz radio frequency of the cyclotron which produced a

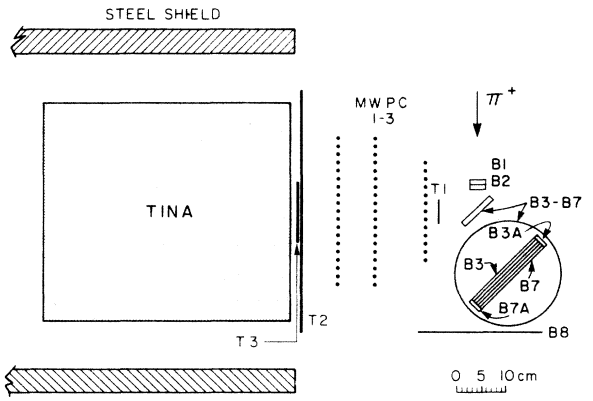

FIG. 1. Experimental setup with details of the stopping counter sandwich $B3$–$B7$ (inset).

~3-ns-wide beam burst on the pion production target every 43.4 ns. The pion stopping counters ($B4$, $B5$, and $B6$) were covered on the upstream and downstream sides by 150-mg cm^{-2} thick scintillators $B3$ and $B3A$ and $B7$ and $B7A$, respectively, to retain the 4.2-MeV muons from pion decays in the target volume. The scintillator sections $B3A$ and $B7A$ were viewed by the same photomultipliers as $B3$ and $B7$, respectively. $B8$ was a large downstream counter used to veto beam particles which passed through the target.

A particle stopping in one of the three inner scintillators was defined by the logic $B1 \cdot B2 \cdot B3 \cdot B4 \cdot (\overline{B7} + \overline{B8})$. A bit-pattern register, gated by the stop signal was used to determine in which scintillator the pion stopped [Fig. 2(a)]. The range width of the stopping pions was 250 mg cm^{-2} full width at half maximum (FWHM) with approximately 30%, 60%, and 10% stopping in $B4$, $B5$, and $B6$, respectively. The positrons from the $\pi \rightarrow e\nu$ decay and from the π-μ-e decay chain were detected by a three-element scintillator telescope ($T1$, $T2$, $T3$) preceding the 46-cm-diameter × 51-cm-long NaI(Tl) crystal TINA at 90° with respect to the beam (see Fig. 1 and Table I). $T3$ limited the positron solid-angle acceptance to $\Delta\omega/4\pi \simeq 0.7\%$ so that the measurements were confined to the central portion of the NaI(Tl) crystal to avoid edge effects and to obtain the best energy resolution.

The signal for a decay positron for the $\pi \rightarrow e\nu$ experiment was a $T1 \cdot T2 \cdot T3$ coincidence. To avoid energy dependence in the event trigger (especially at low energies) a signal from TINA was not required. As a result, the low-energy end of the TINA spectrum contained two peaks—the zero-energy pedestal and the 0.511-MeV positron annihilation γ ray—due to the small fraction of triggers where the positron failed to register in the active volume of the NaI(Tl) crystal. During the early part of the experiment the decay positron detection arm also included three multiwire proportional chambers (MWPC) whose signals were not required in the logic. The MWPC data were used for off-line analysis of position-dependent systematic effects, multiple scattering, etc.

TINA was viewed by seven RCA 4522 photomultipliers. Dynode outputs were passively added at the input of a charge sensitive preamplifier. The preamplifier signal was amplified and shaped with a 250-ns time constant

TABLE I. Counter dimensions in the $\pi e\nu$ experiment (see Fig. 1) (horizontal × vertical × thickness in mm).

Beam scintillators	
$B1$ and $B2$:	30.0 × 30.0 × 9.5
$B3$, $B4$, $B5$, $B6$ and $B7$:	76.2 × 50.8 × 1.6
$B3A$, $B7A$:	8.4 × 50.8 × 1.6
$B8$:	305 × 305 × 3.2
Trigger scintillators	
$T1$:	50.8 diameter × 1.6 or 76.2 diameter × 1.6
$T2$:	483 × 483 × 3.2
$T3$:	127 diameter × 1.6
Multiwire proportional chambers	
MWPC1:	203 × 203
MWPC2 and MWPC3:	305 × 305

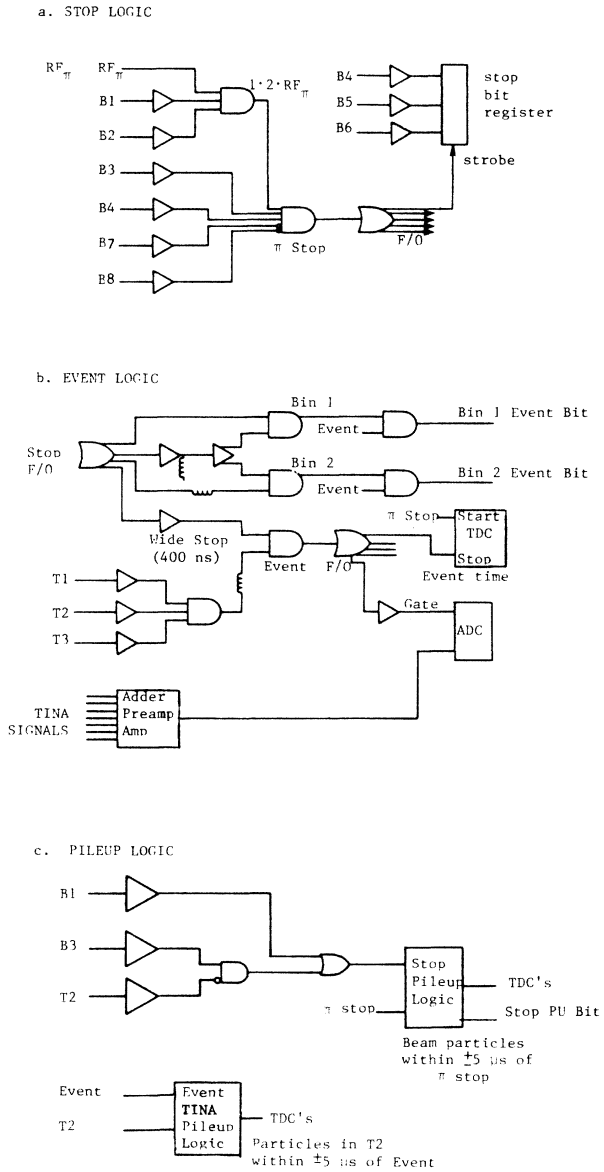

FIG. 2. Schematic of (a) stop logic, (b) event logic, and (c) pileup logic.

and the pulse amplitudes were measured using a 4096 channel analog-to-digital converter (ADC). The tubes viewing the TINA crystal could be selectively removed from the analog sum to equalize gains by adjusting high voltages. The gains of the photomultipliers were monitored using the fitted positions of the zero-energy pedestal, the 0.511-MeV annihilation line and the $\mu \rightarrow e\nu\bar{\nu}$ spectrum. For this purpose the muon-decay positron spectrum was fitted to an empirical function

$$F(C)=\frac{a_1+a_2C+a_3C^2+a_4C^3}{1+\exp[(C-a_5)/a_6]}\ , \tag{4}$$

where C is the channel number, a_1 to a_6 are parameters with a_5 corresponding to the Fermi half-amplitude energy and a_6 being proportional to the resolution.

Figure 2(b) schematically shows the event logic. An event was accepted when there was a $T1\cdot T2\cdot T3$ coincidence within -160 to $+230$ ns of a pion stop. The energy losses (dE/dx) in the scintillators $T1$ to $T3$ were also measured in order to identify positrons. An open-ended delay line placed at the input of a discriminator triggered by the pion stop signal generated two identical 25-ns-long time intervals hereafter called bin 1 and bin 2. Bits were set to flag events occuring during either of the two time bins.

Bin 1 started at $t_i=3$ ns after the pion stop and bin 2 began $t_s=173.4$ ns after t_i corresponding to 4 cyclotron rf periods or 6.7 pion lifetimes. The event time relative to the pion stop was measured using a time-to-amplitude converter and a 8192 channel ADC. The differential nonlinearity of the system was measured several times during the run, using a pulser in random coincidence with a source. The absolute time calibration was measured using the radio-frequency signal from the cyclotron as well as an Ortec 462 time calibrator, with a specified accuracy of $\pm 0.005\%$.

A beam pion preceding or following the current pion stop could disturb the measured time and energy spectra of the events (stop pileup). To detect stop pileup high-threshold discriminators for the counters $B1$ and $B3$ were used (so as not to trigger the pileup logic with beam or decay positrons). The pileup signal was triggered by $B1$ or $(B3\cdot\overline{T2})$. The $B3\cdot\overline{T2}$ requirement was imposed in order to recover events for which the decay positron produced a large pulse in counter $B3$ due to the Landau fluctuations in the positron energy loss. Arrival time of pileup particles was measured with a time-to-digital converter (TDC) if there was a beam pion within ± 5 μs of the current stop. In addition, a bit was set in a register for pileup of beam pions within ± 325 ns of the pion stop.

The TINA energy spectrum could be distorted by additional charged particles close in time to the event (TINA pileup). Counter $T2$ was used to record the charged-particle pileup arrival time in TINA within ± 5 μs of the event. Figure 2(c) shows schematically the stop pileup and the TINA pileup logic. Figures 3(a) and 3(b) show the time distributions and the timing logic sequence for all events.

The data were recorded event by event via CAMAC by a PDP11/34A computer. The following information was recorded for each event: (a) scintillator bit patterns; (b) time of the event relative to the stop; (c) NaI(Tl) pulse height for the event; (d) beam-pion pileup times relative to the pion stop within ± 5 μs (stop pre- and postpileup); (e) $T2$ charged-particle pileup time relative to the event within ± 5 μs (TINA pre- and postpileup); (f) energy-loss information for the scintillators $T1$, $T2$, and $T3$; (g) MWPC 1–3 data.

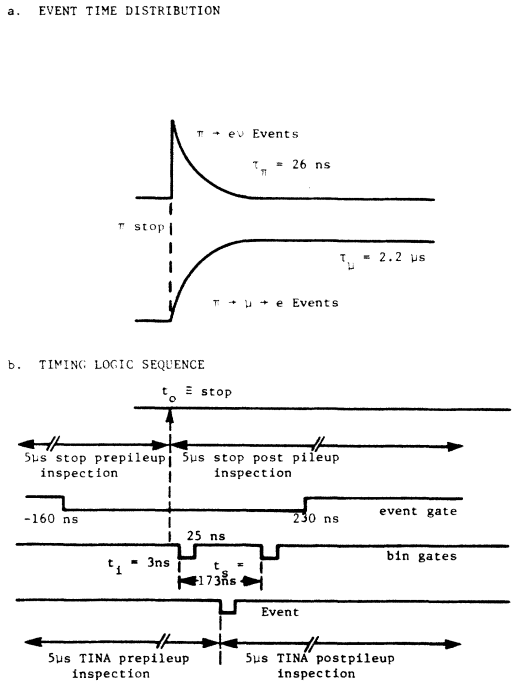

FIG. 3. (a) Event time distribution with respect to the pion stop. (b) Logic time sequence for event with respect to the pion stop.

C. Line-shape measurement

Detailed knowledge of the NaI(Tl) spectrometer response function, including resolution, peak shape, and magnitude of the characteristic low-energy tail, was essential to the data analysis. The response functions were measured separately in a positron beam with momentum spread of $\Delta p/p=1\%$ at 20, 35, 50, 79, and 90 MeV/c. The positron beam was defocused and events were accepted with a radius of 5 cm from the crystal axis corresponding approximately to the acceptance of the $T3$ counter in the $\pi \rightarrow e\nu$ experiment. The energy resolution at 70 MeV/c was $\Delta E/E=3.5\%$ (FWHM). Over the measured energy range, the FWHM width Γ could be well represented by

$$\Gamma\ (\%)=46.3E^{-0.5745},\ E \text{ in MeV}\ . \tag{5}$$

The fractional number of counts in the tail portion of the line shapes corresponding to the region of the $\pi \rightarrow e\nu$ peak lying below the $\mu \rightarrow e\nu\bar{\nu}$ edge was measured at different energies. The result was characterized by an uncertainty of 0.55% due in part to a small contamination of pions and muons in the positron beam for the 70- and 90-MeV/c measurements. Figure 4 shows the measured NaI response function for the 50-MeV/c case.

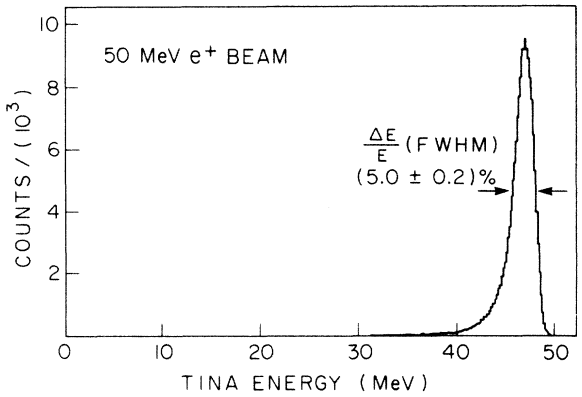

FIG. 4. Measured line shape in the NaI(Tl) crystal TINA for a 50-MeV e^+ beam. The position of the peak (47.2 MeV) is determined by energy loss in the beam scintillators and the insensitive layer in front of the TINA crystal as well as positron annihilation.

III. DATA REDUCTION

To produce a data set suitable for the branching-ratio calculation a number of cuts had to be applied to the raw data.

A. Stop prepileup cut

This cut eliminated those events for which there was a beam particle within a given interval prior to the π stop which triggered the event. Since the μ lifetime is long compared to the π lifetime, increasing the length of the protection interval reduced both the relative number of $\mu \rightarrow e\nu\bar{\nu}$ decay events from previous π stops and the total number of events. The prepileup cut chosen was 525 ns, a compromise between maximizing the total $\pi \rightarrow e\nu$ event rate and minimizing the $\mu \rightarrow e\nu\bar{\nu}$ events from previous pion stops.

B. Stop postpileup cut

The decays of pions which arrived at the target after the trigger stop but within the event acceptance window distorted the shape of the timing spectra. They also produced additional events in bin 2. The probability of a beam pion appearing in the event time window following the trigger stop was 3.5%. The bit set for additional beam pions within ±325 ns of the trigger stop was used to discriminate against stop postpileup events. The efficiency of this cut was studied for its effect on the branching-ratio determination.

C. Event dE/dx cut

Beam pions caused emission of prompt protons via $^{12}C(\pi^+,p)X$ reactions primarily in the $B1$ counter. The observed prompt proton energy spectrum extended to about 90 MeV and these events could distort the energy and time distribution of events. Protons were easily distinguished by their high dE/dx compared to the minimum ionizing positrons. The dE/dx information from the three scintillators $T1$, $T2$, and $T3$ was combined to produce a nearly Gaussian energy-loss spectrum using the minimum pulse theory.[16] The prompt-proton cut applied in this way was estimated to eliminate less than 0.1% of the $\pi \rightarrow e\nu$ events.

D. TINA charged-particle prepileup and postpileup

Additional charged or neutral particles entering the NaI(Tl) crystal before or after the event positron caused energy resolution degradation due to pulse pileup. The pileup cut for charged particles was derived from the $T2$ scintillator covering the entire front face of the crystal. No improvement in the resolution was noted for values of prepileup and postpileup protection intervals larger than 1.5 μs and the cut was set at this value. A small correction to the $\pi \rightarrow e\nu$ branching ratio which resulted from this cut is described in Sec. IV B.

E. Gain correction

A gain correction for signals from TINA was made before obtaining an absolute energy calibration. The relative gain of each run was calculated using the positions of the two low-energy peaks fitted to Gaussians and the $\mu \rightarrow e\nu\bar{\nu}$ energy spectrum fitted to the empirical function of Eq. (4). The gain stability over a two month running period was ±2%. The energy spectra from individual runs were gain-shifted to a standard gain to produce the summed bin-1 and bin-2 energy spectra needed to obtain the tail corrections and to calculate the branching ratio using the two-bin method. Branching ratios were also calculated for the individual runs without gain-shifting as a check of consistency and rate effects. These were found to be in good agreement with the value obtained from the gain-shifted sum.

Gain-shifted data were also used to produce timing spectra for $\pi \rightarrow e\nu$ events above a 52.9-MeV cutoff energy and for $\mu \rightarrow e\nu\bar{\nu}$ events below this energy. These spectra were used in the second calculation of the branching ratio using the timing fits.

IV. DATA ANALYSIS AND RESULTS

A. Energy calibration and tail correction

Energy calibration required detailed analysis of bin-1 and bin-2 energy spectra. Figure 5(a) shows the spectrum of positron energy deposited in the NaI(Tl) crystal for bin 1 including the $\pi \rightarrow e\nu$ peak and the $\mu \rightarrow e\nu\bar{\nu}$ spectrum. It extends to zero-observed energy since the NaI(Tl) pulse was not required in the event logic. The expanded low-energy region shown in Fig. 5(b) reveals the two low-energy peaks due to the zero-energy ADC pedestal and the 0.511-MeV positron annihilation line. These two peaks were due to positrons which stopped in $T3$ or in the insensitive front layer of TINA consisting of 1.6 mm of Al, 0.3 mm CH_2, and 1.6 mm of packed MgO (reflective layer). Figure 5(c) gives the pure $\mu \rightarrow e\nu\bar{\nu}$ spectrum from bin 2.

To obtain the branching ratio the number of π-μ-e events in bins 1 and 2 and the total number of $\pi \rightarrow e\nu$ events in bin 1 are required. For the $\pi \rightarrow e\nu$ events a

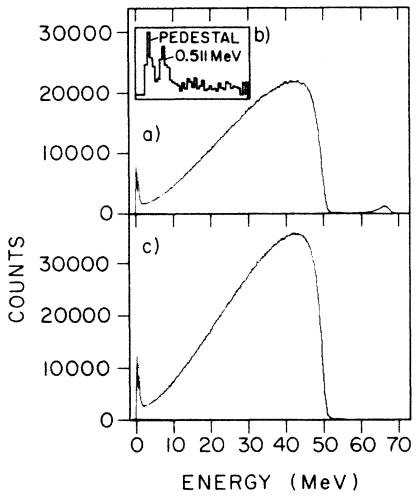

FIG. 5. (a) Positron energy spectrum for events in bin 1. (b) Expanded-scale low-energy region for bin 1. (c) Positron energy spectrum for events in bin 2.

correction must be made for the small fraction of events which fall under the π-μ-e spectrum due to radiative processes, to the NaI(Tl) resolution function with its characteristic low-energy tail, and to energy loss for the beam-target-detector geometry. Since the tail correction corresponded to approximately 1.5% of the total number of $\pi\to e\nu$ events below 51 MeV it was crucial to estimate it carefully. This calculation relied on the detailed knowledge of the NaI line shape for the $\pi\to e\nu$ events and on the energy calibration. Both were obtained by using Monte Carlo generated empirical $\pi\to e\nu$ and $\mu\to e\bar{\nu}\nu$ line shapes.

Figure 6 shows the experimental $\pi\to e\nu$ bin-1 spectrum obtained by subtracting the normalized bin 2 $\mu\to e\bar{\nu}\nu$ spectrum from bin 1. Also shown is the fit to the data using the Monte Carlo generated $\pi\to e\nu$ line shape. The χ^2 is 1.01 per degree of freedom indicating that no important effects have been overlooked. The measured peak width of $\Delta E/E=5.5\%$ is in agreement with the Monte Carlo calculation. There are $N_{\pi e}=3.2\times10^4$ counts in the peak with $E>51$ MeV.

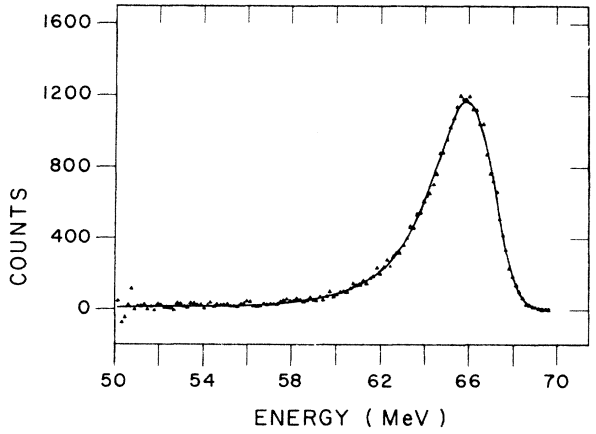

FIG. 6. Fit to the $\pi\to e\nu$ line with the Monte Carlo–generated line shape.

To determine the empirical $\pi\to e\nu$ Monte Carlo line shape, pions were simulated to stop in the target according to the measured range curve (FWHM=250 mg cm^{-2} centered 60 mg cm^{-2} upstream of the target center). For the experimental geometry, $\pi\to e\nu$ decay positrons were traced from the target to the NaI(Tl) crystal allowing for $\pi\to e\nu\gamma$ inner-bremsstrahlung radiative corrections,[17] Landau energy-loss fluctuations, and Bhabha scattering. The total energy deposited in the crystal was obtained by summing the kinetic energy of the detected positron, positron annihilation energy (1.02 MeV), and the energies of any detected radiative photons and Bhabha scattered electrons. This energy spectrum was then numerically convoluted with the measured crystal resolution functions using Eq. (5) for interpolation to produce the empirical $\pi\to e\nu$ line shape used to fit the experimental $\pi\to e\nu$ data.

The empirical shape for the $\mu\to e\bar{\nu}\nu$ spectrum was obtained from a Monte Carlo calculation similar to the one for the $\pi\to e\nu$ events. Pions stopped in the target according to the measured range curve. The 4.2-MeV muons from the pion decay were contained in the target region and were allowed to decay into electrons. As with $\pi\to e\nu$ events, a spectrum containing the various simulated physical processes was produced including $\mu\to e\bar{\nu}\nu\gamma$ radiative corrections[18] for the experimental geometry. This line shape was convoluted with the measured NaI(Tl) resolution functions to produce the empirical Monte Carlo $\mu\to e\bar{\nu}\nu$ spectrum shape.

Acceptable fits to both the bin-1 and bin-2 $\mu\to e\bar{\nu}\nu$ spectra could only be obtained by excluding the pileup region above 49 MeV and the low-energy region below 5 MeV where the energy loss and resolution uncertainties were large. The fit provided adequate energy information for the $\mu\to e\bar{\nu}\nu$ spectrum needed for energy calibration. The energy calibration of the data, given in Table II, was obtained by making a least-squares fit to the $\pi\to e\nu$ peak, the $\mu\to e\bar{\nu}\nu$ spectrum and the two low-energy peaks. The branching-ratio determination was insensitive to the distortions in the $\mu\to e\bar{\nu}\nu$ spectrum since only the total number of counts is used as discussed below.

An estimate for the magnitude of the two low-energy peaks including the effects of multiple scattering gave (0.55±0.20)% of the total number of counts in the $\mu\to e\bar{\nu}\nu$ spectrum. This was in good agreement with the measured values of (0.725±0.004)% and (0.710±0.003)% for bins 1 and 2, respectively. The small excess of counts

TABLE II. Monte Carlo fits to the $\pi\to e\nu$ data, $\mu\to e\bar{\nu}\nu$ decay spectrum, low-energy peaks and the energy calibration.

Quantity	Calibrated energy (MeV)	Monte Carlo energy (MeV)	ΔE (MeV)
$\pi\to e\nu$ peak	65.90	65.88	0.020
$\pi\to e\nu$ width	3.36	3.43	−0.065
$\mu\to e\bar{\nu}\nu$ peak	41.78	41.73	0.049
$\mu\to e\bar{\nu}\nu$ width	28.63	28.46	0.169
Pedestal	0.027	0.0	0.027
e^+ annihilation radiation	0.477	0.511	−0.034

E_{calib} (MeV) $= -3.78 + 0.14981\times$channel

in the low-energy peaks in bin 1 over bin 2 has been estimated to be due to Compton scattering of the γ's from $\pi \to \mu\nu\gamma$ decays in the target material.

B. Branching ratio using the two-bin method

The total number of $\pi \to e\nu$ events was obtained by calculating the number of events above a cutoff energy E_c and applying a tail correction below this energy using the Monte Carlo–generated line shape. In order to assess the reliability of the tail correction, it was calculated as a function of E_c. The stability of the branching ratio obtained as E_c was varied indicated the validity of the tail correction. The energy spectrum was divided into the $\pi \to e\nu$ region above E_c and the $\mu \to e\nu\bar{\nu}$ region below E_c. A fraction p of the $\pi \to e\nu$ counts was below E_c due to the tail of the $\pi \to e\nu$ line shape and a fraction q of the $\mu \to e\nu\bar{\nu}$ counts was above E_c due to pileup effects in the energy spectra. We further defined for the two bins ($i=1,2$) total $\pi \to e\nu$ region counts n_i, total π-μ-e region counts m_i, net $\pi \to e\nu$ counts a_i and net π-μ-e counts b_i, with λ_π, λ_μ, and t_s having been defined earlier (Sec. II A). It can be shown that

$$a_1=(m_2n_1-m_1n_2)/\{m_2(1-p)-pn_2e^{-\lambda_\pi t_s} \times[m_1(1-p)-n_1p]\}\ , \tag{6}$$

$$b_1=n_1+m_1-a_1\ , \tag{7}$$

$$b_2=n_2+m_2-a_1e^{-\lambda_\pi t_s}\ . \tag{8}$$

Then the tail-corrected branching ratio becomes

$$R_1=\frac{a_1}{e^{\lambda_\mu t_s}b_2-b_1}\frac{\lambda_\mu}{\lambda_\pi-\lambda_\mu}(1-e^{-t_s(\lambda_\pi-\lambda_\mu)})\ . \tag{9}$$

There are two conflicting requirements in applying the tail corrections. Ideally E_c should be as low as possible in order to apply the least correction. Unfortunately, lowering E_c increases the $\mu \to e\nu\bar{\nu}$ contamination to be subtracted from under the $\pi \to e\nu$ events leading to increased statistical uncertainty. A compromise was reached at $E_c=51$ MeV from these considerations and the stability of the branching ratio as a function of E_c. The uncertainty in the tail correction due to the choice of the cutoff energy was estimated to be 0.51%. When combined with the earlier uncertainty of 0.55% in the measured NaI(Tl) resolution function, this led to a total uncertainty of 0.75%. The overall tail correction applied to the branching ratio was (1.47±0.75)%.

Several other corrections shown in Table III were applied to the tail-corrected branching ratio to obtain the final branching ratio. These were obtained from Monte Carlo calculations or from detailed analysis of data. The accuracy in evaluation of these corrections is affected by the uncertainties in the geometry for the target, scintillators, and the NaI(Tl) detector. These corrections are discussed below.

After the tail correction, effects of multiple scattering led to the next largest uncertainty. Multiple Coulomb scattering is an energy-dependent process in which positrons may be scattered into or out of the acceptance. A Monte Carlo simulation based on Moliere theory corrected[19] for finite scattering angles ($\sin\theta \neq \theta$) was done. As a check the calculation reproduced existing precise measurements of multiple scattering of low-energy electrons in gold and beryllium.[20] For the $\pi \to e\nu$ and $\mu \to e\nu\bar{\nu}$ events the program kept track of the number of particles scattered into or out of the acceptance. Calculations were repeated for variations in the beam-target-detector geometry to determine the effect of uncertainties in the geometry. From these calculations a multiplicative correction factor due to multiple scattering of 0.9977±0.0040 for the branching ratio was obtained.

TABLE III. Multiplicative corrections to $\pi \to e\nu$ branching ratio obtained by the two-bin method.

$\pi \to e\nu$ tail	1.0147±0.0075
Low-energy $\mu \to e\nu\nu$	0.9982±0.0005
Multiple Coulomb scattering	0.9977±0.0040
Positron annihilation	0.9959±0.0010
Bin-1 and bin-2 equality	0.9989±0.0004
Pileup correction	0.9931±0.0029
Pion lifetime	1.0000±0.0009
Pion-muon solid-angle difference	0.9986±0.0011
π-μ decay false veto in target	1.0002±0.0010
Positron false veto in target ($B7A$ lip)	1.0018±0.0017

Some of the positrons annihilated in the scintillators before reaching the NaI(Tl) crystal. The energy-dependent annihilation cross section was taken from Heitler.[21] The difference in the annihilation for $\pi \to e\nu$ events and $\mu \to e\nu\bar{\nu}$ events led to a multiplicative correction factor of 0.9959±0.0010 for the branching ratio. Some of the low-energy positrons from the $\mu \to e\nu\bar{\nu}$ decay were lost from the trigger due to low range. These led to a trigger-loss correction factor of 0.9982±0.0005.

The branching-ratio determination depends on precise equality of the two time bins. A measurement of the two bin widths by counting a radioactive source in random coincidence with a pulser indicated a small difference which led to a branching-ratio correction of (0.9989±0.0004). The 100-ps uncertainty in the measured bin separation t_s had a negligible effect on the branching ratio.

There were three small corrections required to account for aspects of the target configuration. A factor of 0.9986±0.0011 accounted for the effect of a difference in solid angle for $\mu \to e\nu\bar{\nu}$ events and $\pi \to e\nu$ events due to the fact that the 4.2-MeV decay muons occupy a slightly larger volume in the target than the original pions. Although it was determined that all the decay muons from stopped pions were contained within the total target volume, it was possible for a fraction of pions to decay to muons which entered the veto counter $B7$. The resulting false stop veto signals caused a small loss of stops and required a correction factor of 1.0002±0.0010. Parts of the last segment of the target ($B7A$ lip—see Fig. 1) could intercept a fraction of the solid angle for positrons from both $\pi \to e\nu$ and $\mu \to e\nu\bar{\nu}$ decay. At early time (<10 ns) this could lead also to lost events due to a false stop veto in the target. The correction for this was 1.0018±0.0017.

The effects of the pileup cuts on the branching ratio were determined by using different sets of pileup conditions in the analysis and from measured inefficiencies of the counters. The following effects were included.

(i) Inefficiencies in the detection of stop postpileup.

(ii) A small distortion in the bin-1 and bin-2 event ratio due to the fact that the rate of TINA pileup depended on the counter $T2$ rate which varied with time after the pion stop.

(iii) A fraction of the stop postpileup signals were false because they were generated by a stopped pion in counter $B4$ that decayed into a muon which could enter the active volume of counter $B3$ and trigger the postpileup logic.

The resulting overall correction factor from the pileup effects was 0.9931 ± 0.0029. Finally, the uncertainty in the measured pion lifetime[22] $\tau_\pi=1/\lambda_\pi=26.030\pm0.023$ ns contributed a correction factor of 1.0000 ± 0.0069 to the branching ratio.

Including the corrections listed in Table III the final value of the branching ratio based on the data shown in Fig. 5 and Eq. (9) is

$$R=(1.218\pm0.014)\times10^{-4}\,. \tag{10}$$

C. Branching ratio using the timing method

The second method for determining the branching ratio made use of the data shown in the two timing spectra in Fig. 7. Events which occurred prior to the arrival of the pion ($t=0$) were due to decays of muons left in the target by previous pion stops. The time distributions included all events in the π-μ-e energy region [Fig. 7(a)] and in the $\pi\to e\nu$ peak region [Fig. 7(b)] over a wider time range than just bins 1 and 2.

The full expression used to fit the timing spectra included a muon contamination in the pion beam and small corrections to account for the effects of the pileup circuitry. The function for events below $E_c=52.9$ MeV due mostly to the π-μ-e decay chain was

$$f_{\pi\mu e}(t)=N\left[\theta(t)[(1-q-R)\phi(t)+Rp\lambda_\pi e^{-\lambda_\pi t}+\alpha_1\lambda_\mu e^{-\lambda_\mu t}]-\theta(t-t_F)\alpha_2\phi(t-t_F)\right.$$
$$\left.+\sum_{\substack{n=-8\\ n\neq0}}^{8}\theta(t-t_{rf}n)\phi(t-t_{rf}n)\alpha_3+\alpha_4\lambda_\mu e^{-\lambda_\mu t}\right]\,. \tag{11}$$

The expression for $\pi\to e\nu$ decay events above the cutoff energy E_c was

$$f_{\pi e}(t)=N\left[\theta(t)[R(1-p)\lambda_\pi e^{-\lambda_\pi t}+q\phi(t)]+\alpha_3R\sum_{\substack{n=-8\\ n\neq0}}^{8}\theta(t-t_{rf}n)\lambda_\pi e^{-\lambda_\pi(t-t_{rf}n)}+\alpha_5\lambda_\mu e^{-\lambda_\mu t}\right]\,, \tag{12}$$

where $\theta(t)=0$ for $t\leq0$ ns and $\theta(t)=1$ otherwise.

Here N is the total number of pion decays, R the branching ratio to be determined and the function $\phi(t)$ describes the sequential π-μ-e decay-chain time distribution

$$\phi(t)=\frac{\lambda_\pi\lambda_\mu}{\lambda_\pi-\lambda_\mu}(e^{-\lambda_\mu t}-e^{-\lambda_\pi t})\,. \tag{13}$$

The tail of the NaI(Tl) response function caused a fraction p of the $\pi\to e\nu$ counts below E_c to be included in the function $f_{\pi\mu e}(t)$. Similarly, resolution and pileup effects in the energy spectrum caused a fraction q of π-μ-e events above E_c to be included in the function $f_{\pi e}(t)$. The parameter α_1 accounted for the muon component in the beam.

Pileup effects were explicitly included in the fitting functions. A fraction α_2 of the pions stops in the counter $B4$ could decay to muons stopping in $B3$ and caused a false stop pileup. The retriggering time for this process was $t_F\sim28$ ns.

The terms with α_3 accounted for the inefficiency of the stop pileup circuitry for beam pions in the subsequent rf cycles spaced $t_{rf}=43.4$ ns apart. The α_4 and α_5 terms ac-

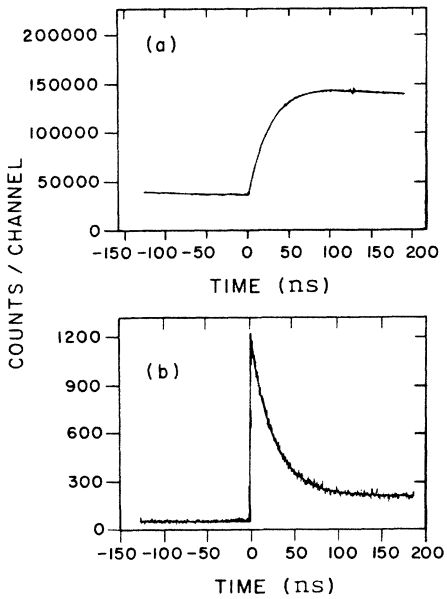

FIG. 7. Time distribution for (a) events below $E_c=52.9$ MeV and (b) events above E_c. Solid lines are fits to the data.

counted for muon decays from previous pions stopping before the prepileup cut of 525 ns (Sec. III A).

In addition, two small corrections [not indicated in Eqs. (11) and (12)] arising from events incorrectly vetoed by the edge of counter $B7$ ($B7A$ lip veto) and TINA pileup correction were introduced into both π-μ-e and $\pi \to e\nu$ time spectra. The multiplicative correction term from the $B7A$ lip veto was $h(t)=0.999$ for -7 ns $\leq t \leq 7$ ns and $h(t)=1.000$ otherwise, applied to $f_{\pi\mu e}$ and $f_{\pi e}$. The effect of TINA pileup required a correction factor of $1-0.004e^{-\lambda_\mu t}$ for the $\pi \to e\nu$ and π-μ-e components. The correction factor was $1+0.03e^{-\lambda_\mu t}$ for the muons. (See pileup corrections, Sec. IV B.)

The timing spectra of π-μ-e and $\pi \to e\nu$ events were fitted simultaneously using a fitting program, MINUIT.[23] Free parameters were the number of π decay events N, the muon decay terms α_4 and α_5, the branching ratio R, the fraction q of π-μ-e events above E_c, and the zero time (t_0) which was introduced by replacing $t-t_0$ for t in Eqs. (11) and (12). The π and μ lifetimes were set at the currently accepted values of 26.03 and 2197.3 ns, respectively. The tail correction p for $\pi \to e\nu$ events below E_c was set at 0.021 as determined from the line-shape analysis. The amplitude arising from the μ contamination in the beam α_1 was set to be zero based on an estimation of $<0.3\%$ from the time-of-flight (TOF) spectrum of the incident particles for the analyzed events. Based on separate analysis, the $B3$ false stop pileup correction α_2 was fixed at -0.00475 and the stop pileup inefficiency correction α_3 was set at 0.00024 which is a product of the measured inefficiency of the scintillators and the probability of having random incident particles. Errors due to uncertainties in the fixed parameters were estimated by varying each parameter and are included in Table IV.

To estimate systematic effects, a term with time dependence $e^{-2\lambda_\mu t}$ was introduced as additional background. Terms with this time dependence arise in second order from TINA pileup corrections. A small but statistically significant component with this time dependence was found, and about 20% of it could be accounted for from the TINA pileup correction. The source of the remainder is unknown. The introduction of this component led to an increase of 0.3% in the branching ratio.

In the study of systematic effects, several fixed parameters were also set free in the fits. The maximum variation of the branching ratio was 0.4% which happened when the $B3$ false stop pileup converged to $\alpha_3=0.0001$. The difference of the branching ratio between the fits with free and fixed pion lifetime was 0.1%. The dependence on the fitting region was studied by varying the regions for the fit. This resulted in an uncertainty of 0.3% in the branching ratio. Close inspection of Fig. 7(a) shows an anomalous distortion in the time region near 120 ns. The difference between the values of R calculated including and excluding the anomalous distortion (wiggle) region was about 0.1%. The χ^2/DF was 1.6 when the wiggles were in the fit and 1.2 when they were excluded.

In addition to the fitting procedure, certain of the multiplicative corrections determined for the two-bin method (Sec. IV B) must be applied to the result. The corrections applicable, listed in Table IV, are low-energy π-μ-e trigger losses, the pion-muon solid-angle difference, $\pi \to \mu\nu$ decay

TABLE IV. Corrections and uncertainties for $\pi e\nu$ branching ratio determination from time spectra.

Fixed parameters in fit	Magnitude	Corresponding uncertainty in R
Tail correction p	0.021	±0.75%
μ contamination in beam, α_1	0.00	±0.06%
$B3$ false stop pileup, α_2	−0.00475	±0.3%
Stop pileup inefficiency, α_3	0.00024	<0.1%
Positron false veto in target ($B7A$ lip)	0.999 ($-7 \leq t \leq 7$ ns) 1.000 (otherwise)	<0.1%
TINA pileup	$1-0.004\,e^{-\lambda_\mu t}$ (π-μ-e,πe) $1+0.03e^{-\lambda_\mu t}$ (muons)	±0.06%
Multiplicative corrections to R		
Low-energy $\mu \to e\bar{\nu}\nu$ loss	0.9982	±0.05%
Pion-muon solid-angle difference	0.9986	±0.11%
$\pi \to \mu\nu$ decay false veto in target	1.0002	±0.10%
Multiple Coulomb scattering	0.9977	±0.40%
Positron annihilation	0.9959	±0.10%
Fitting procedure		
Anomalous distortion at ~120 ns		±0.10%
Fitting region included		±0.30%
Unknown background		±0.30%

false veto in the target, multiple scattering, and positron annihilation. Including all the above corrections, the branching ratio determined from the timing method is

$$R=(1.219\pm0.014)\times10^{-4} \quad (14)$$

and is consistent with the result of Eq. (10).

D. Pion lifetime

During the validity test of the expression for the timing fit, a pion lifetime was deduced from the same spectrum that was used in the study of the branching ratio. When the pion lifetime was left as a free parameter in the fit a value of 26.10±0.05 ns including only a statistical error, was obtained in good agreement with the currently accepted value[22] of 26.030±0.023 ns. This helped to confirm the validity of the fitting expression. To estimate the systematic uncertainties in this number, the effect of uncertainties in the other parameters was studied by varying their values. Since the timing spectrum around t_0 (π stop) was disturbed by the introduction of pileup cuts (a typical example is the $B3$ stop pileup), there seemed to be a slight dependence on the fitting region. This was also true in the determination of the branching ratio as mentioned in the previous section. The uncertainty due to different fitting regions was estimated to be 0.11 ns from the fits for different regions. The error from the uncertainty of the $B3$ false pileup was 0.04 ns. The contributions from other fixed parameters, such as the muon contamination in the beam, were negligible. The pion lifetime obtained by combining these uncertainties in quadrature is 26.10±0.13 ns.

V. CONCLUSIONS

The result for the branching ratio of Eq. (10) [or Eq. (14)] is in good agreement with the predictions of the standard model of weak and electromagnetic interactions with the assumption of electron-muon universality. A quantitative test of universality can be obtained by writing Eq. (1) as

$$R=1.233(f_\pi^e/f_\pi^\mu)^2\times10^{-4}$$
$$=(1.218\pm0.014)\times10^{-4}, \quad (15)$$

where f_π^l is the pion decay constant. Then

$$f_\pi^e/f_\pi^\mu=0.9939\pm0.0057, \quad (16)$$

where a value of unity corresponds to perfect universality. This test of e-μ universality is unaffected by the uncertainty in the $\pi\to e\nu$ branching ratio due to pion-structure-dependent effects.[24]

The branching ratio is very sensitive to the contribution of a pseudoscalar coupling to π_{l2} decay because decays via this mechanism are not helicity suppressed. The resulting limit on the pseudoscalar coupling contributing to the π_{l2} decay is

$$f_p=(-0.0061\pm0.0057)f_\pi m_e . \quad (17)$$

Pseudoscalar currents arise in many extensions of the standard model.[9] In many models with charged Higgs particles, the Yukawa coupling between the Higgs boson and the fermions is simply proportional to a heavy-fermion mass, e.g., M_τ. Using the formulation of Shanker,[9] a lower-mass bound for charged Higgs particles resulting from the present experiment is $M_{H^+}>350$ GeV assuming maximal couplings. However, the $\pi\to e\nu$ branching ratio is not affected for charged-Higgs-boson—fermion coupling proportional to the lepton mass as in the standard model. Other mass bounds can be set for pseudoscalar leptoquarks (>700 GeV) which occur in models with dynamical symmetry breaking such as hypercolor theories, and for vector leptoquarks (>90 TeV) in the Pati-Salam type of grand unified theories.[9]

ACKNOWLEDGMENTS

We wish to thank G. Mason, W. Sperry, and D. Berghofer for their participation in an early phase of this work, and C. K. Hargrove, H. Fearing, and C. E. Picciotto for many helpful discussions. We wish to thank J. Ng for his encouragement and helpful discussions and B. C. Robertson for his participation in the data-taking phase of this work. The experiment was funded in part by the Natural Sciences and Engineering Research Council of Canada.

---

*Also at University of Victoria, Victoria, British Columbia, Canada.
†Mailing address: Stanford Linear Accelerator Center, Stanford CA 94305.
‡Present address: University of Ife, Ile-Ife, Nigeria.
§Also at University of British Columbia, Vancouver, British Columbia, Canada.

[1]M. Ruderman and R. Finkelstein, Phys. Rev. **76**, 1458 (1949).
[2]T. Fazzini *et al.*, Phys. Rev. Lett. **1**, 247 (1958); G. Impeduglia *et al.*, *ibid.* **1**, 249 (1958).
[3]W. J. Marciano and A. Sirlin, Phys. Rev. Lett. **36**, 1425 (1976); See also D. A. Bryman, P. Depommier, and C. Leroy, Phys. Rep. **88**, 153 (1982).
[4]S. M. Berman, Phys. Rev. Lett. **1**, 468 (1958).
[5]T. Kinoshita, Phys. Rev. Lett. **2**, 477 (1959).
[6]T. Goldman and W. J. Wilson, Phys. Rev. D **15**, 709 (1977).
[7]J. A. Jaros *et al.*, Phys. Rev. Lett. **51**, 955 (1983).
[8]M. Kobayashi and T. Maskawa, Prog. Theor. Phys. **49**, 652 (1973).
[9]H. E. Haber, G. L. Kane, and T. Sterling, Nucl. Phys. **B161**, 493 (1979); J. F. Donoghue and L.-F. Li, Phys. Rev. D **19**, 945 (1979); B. McWilliams and L.-F. Li, Nucl. Phys. **B179**, 62 (1981); O. Shanker, *ibid.* **B204**, 375 (1982); K. Mursula, M. Roos, and F. Scheck, *ibid.* **B219**, 321 (1983).
[10]R. E. Shrock, Phys. Rev. D **24**, 1232 (1981).
[11]D. A. Bryman *et al.*, Phys. Rev. Lett. **50**, 1546 (1983).

[12]H. L. Anderson *et al.*, Phys. Rev. **119**, 2050 (1960).
[13]E. Di Capua *et al.*, Phys. Rev. **133**, B1333 (1964).
[14]D. Bryman and C. Picciotto, Phys. Rev. D **11**, 1337 (1975).
[15]D. A. Bryman *et al.*, Phys. Rev. Lett. **50**, 7 (1983).
[16]K. Nagata, Nucl. Instrum. Methods **77**, 218 (1970).
[17]S. G. Brown and S. A. Bludman, Phys. Rev. **136**, B1160 (1964).
[18]C. Fronsdal and H. Uberall, Phys. Rev. **113**, 654 (1959); See also G. Källen, in *Radiative Corrections in Elementary Particle Physics,* edited by G. Höhler (Springer Tracts in Modern Physics, Vol. 46) (Springer, Berlin, 1968), p. 67.
[19]H. A. Bethe, Phys. Rev. **89**, 1256 (1953); See also W. T. Scott, Rev. Mod. Phys. **35**, 231 (1963).
[20]A. O. Hanson *et al.*, Phys. Rev. **84**, 634 (1951).
[21]W. Heitler, *Quantum Theory of Radiation* (Clarendon, Oxford, 1954).
[22]Particle Data Group, Rev. Mod. Phys. **56**, S91 (1984).
[23]F. James and M. Roos, MINUIT, CERN Report No. DD/75/20, 1975 (unpublished).
[24]Since there are theoretical uncertainties in the pion structure-dependent radiative corrections, their effect is not included in the experimental and theoretical branching ratios quoted in the text. Using the conserved-vector-current hypothesis, the rate for the structure-dependent $\pi \to e\nu\gamma$ process has been parametrized (see Ref. 3) in terms of the π^0 lifetime and h, the ratio between the vector and the axial-vector pion weak form factors. At present, there are two possible experimental values of h, -2.36 ± 0.12 and 0.44 ± 0.12. For $h=-2.36$ the theoretical expectation of Eq. (1) would become $R_{\text{theory}}=1.238\times10^{-4}$ and the experimental result would be increased to $R_{\text{expt}}=(1.223\pm0.014)\times10^{-4}$ to take account of unobserved events with $E_e<51$ MeV due to the structure-dependent radiation. For $h=0.44$, $R_{\text{theory}}=1.234\times10^{-4}$ and $R_{\text{expt}}=(1.218\pm0.014)\times10^{-4}$. Thus the difference between the theory and the experiment remains unaltered.

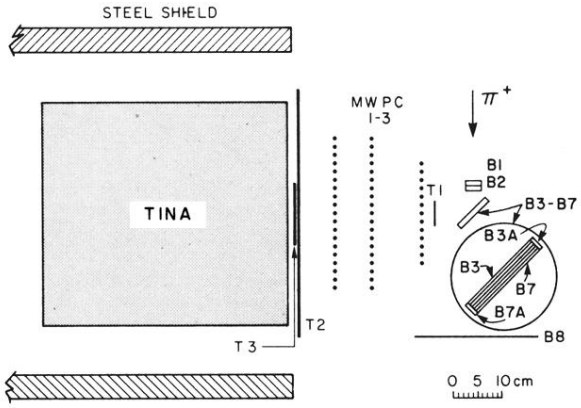

FIG. 1. Experimental setup with details of the stopping counter sandwich $B3$–$B7$ (inset).